Limits on wCDM from the EFTofLSS with the PyBird code

Guido D'Amico¹, Leonardo Senatore^{2,3}, Pierre Zhang^{4,5,6}

- ¹ Dipartimento di SMFI dell' Universita' di Parma & INFN Gruppo Collegato di Parma, Parma, Italy
 - ² Stanford Institute for Theoretical Physics, Physics Department, Stanford University, Stanford, CA 94306
 - ³ Kavli Institute for Particle Astrophysics and Cosmology, SLAC and Stanford University, Menlo Park, CA 94025
 - ⁴ Department of Astronomy, School of Physical Sciences, University of Science and Technology of China, Hefei, Anhui 230026, China
 - ⁵ CAS Key Laboratory for Research in Galaxies and Cosmology, University of Science and Technology of China, Hefei, Anhui 230026, China
 - ⁶ School of Astronomy and Space Science, University of Science and Technology of China, Hefei, Anhui 230026, China

Abstract We apply the Effective Field Theory of Large-Scale Structure to analyze the wCDM cosmological model. By using the full shape of the power spectrum and the BAO post-reconstruction measurements from BOSS, the Supernovae from Pantheon, and a prior from BBN, we set the competitive CMB-independent limit $w = -1.046^{+0.055}_{-0.052}$ at 68% C.L.. After adding the Planck CMB data, we find $w = -1.023^{+0.033}_{-0.030}$ at 68% C.L.. Our results are obtained using PyBird, a new, fast Python-based code which we make publicly available.

1 Introduction and Summary

Introduction: After a long journey, the Effective Field Theory of Large-Scale Structure (EFtofLSS) has been recently applied to the power spectrum of the galaxies of BOSS/SDSS [1, 2, 3 ¹. These results have allowed us to measure all the cosmological parameters of the $\nu\Lambda \text{CDM}$ model, except neutrino masses, just using a prior from Big Bang Nucleosynthesis (BBN). The smallness of the error bars on some of these parameters have shown the power of Large-Scale Structure (LSS) surveys even without the inclusion of any cosmic microwave background (CMB) prior. For example, the constraint on the present-day dark matter fraction, Ω_m , is competitive with the one from Planck2018 [4], and the one on the present-day Hubble parameter, H_0 is measured with the same precision as the one measured from Cosmic Distance Ladder, such as SH0ES [5]. Since the results from [1, 2, 3] are compatible with Planck, they contribute to shed light on the so-called Hubble tension (see a review in [6]). Though the number of modes in BOSS is much smaller than the ones in Planck, the origin of these remarkable results lies mainly in the fact that the CMB and LSS observables depend quite differently on the cosmological parameters, so that degeneracies are different (see for example sec. 4.3 of [1]). Most importantly, these results show that the contribution of next generation LSS surveys, once analyzed with a controlled theory such as the EFTofLSS, to our understanding of the history of the universe might be much larger than what previously believed, potentially helping to continue the remarkable exploration that was achieved in the past decades.

As mentioned, the application of the EFTofLSS to data is the result of a long journey where each of the ingredients of the EFTofLSS that was required in order to be able to apply it to data was one-by-one subsequently developed, tested on simulations, and shown to be successful. Though not all those intermediate results are directly used in the analysis, they were *necessary* for us, and probably for anybody else, to apply the model to data. We therefore find it fair, in each instance where the EFTofLSS is applied to data, to add the following footnote where we acknowledge at least a fraction of those most important developments ².

¹Notice that Ref. [3] is a companion paper to [1]. Ref. [1] also applied it to the bispectrum, but finding marginal improvements, probably due to the fact that only the tree-level prediction was being used, so that the k-reach was not quite high.

²The initial formulation of the EFTofLSS was performed in Eulerian space in [7, 8], and subsequently extended to Lagrangian space in [9]. The dark matter power spectrum has been computed at one-, two-and three-loop orders in [8, 10, 11, 12, 13, 14, 15, 16, 17, 18, 19]. These calculations were accompanied by some theoretical developments of the EFTofLSS, such as a careful understanding of renormalization [8, 20, 21] (including rather-subtle aspects such as lattice-running [8] and a better understanding of the velocity field [10, 22]), of the several ways for extracting the value of the counterterms from simulations [8, 23], and of the non-locality in time of the EFTofLSS [10, 12, 24]. These theoretical explorations also include an enlightening study in 1+1 dimensions [23]. An IR-resummation of the long displacement fields had to be performed in order to reproduce the BAO peak, giving rise to the so-called IR-Resummed EFTofLSS [25, 26, 27, 28, 29]. An account for baryonic effects was presented in [30]. The dark-matter bispectrum has been computed at one-loop in [31, 32], the one-loop trispectrum in [33], the displacement field in [34]. The lensing power spectrum has been computed at two loops in [35]. Biased tracers, such as halos and galaxies, have been studied in the context

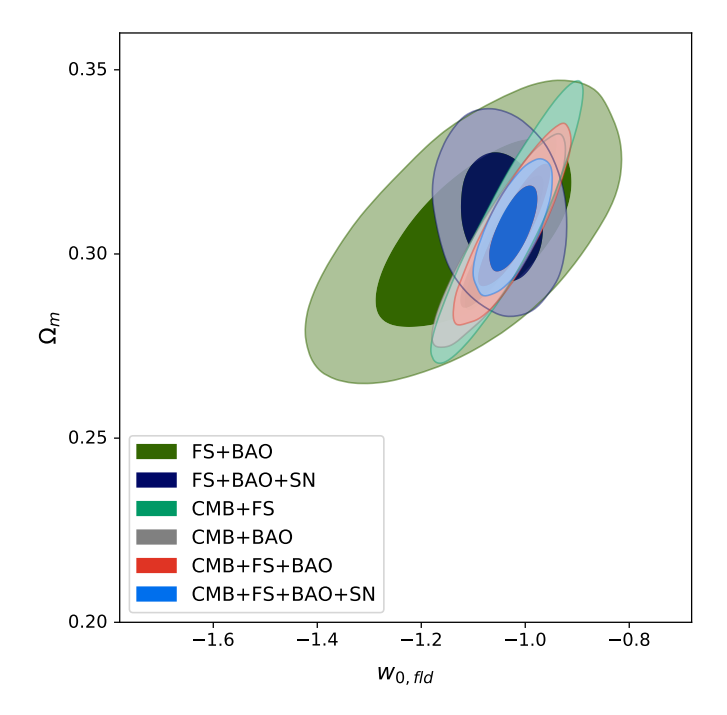


Figure 1: $w - \Omega_m$ contour from the various analyses performed in this work. When not analyzed in combination with CMB, we always use a BBN prior. These results show the power of LSS, when analyzed with the EFTofLSS approach at long wavelengths, to constrain dark energy.

Data sets: In this paper we focus on applying the EFTofLSS to analyze the wCDM model. We analyze various combinations among the full shape (FS) of BOSS DR12 pre-reconstructed power spectrum measurements [53], baryon acoustic oscillations (BAO) of BOSS DR12 post-reconstructed power spectrum measurements [54], Planck2018 TT,TE,EE+lowE + lensing [4]. We also consider combinations with Supernovae (SN) measurements from the Pantheon Sample [55]. When quoting BAO, we also include measurements at small redshift from 6DF [56] and SDSS DR7 MGS [57], as well as high redshift Lyman- α forest auto-correlation and cross-correlation with quasars from eBOSS DR14 measurements [58, 59]. The inclusion of post-reconstructed BAO measurements gives a non-negligible improvement because the reconstruction amounts to using higher n-point functions. However the pre- and post-reconstruction BAO measurements are correlated. We describe how we account for this in App. A (see also [60]). When combined with Planck or SN, we simply add the log-likelihoods, since all the measurements refer to separate redshift bins. There is a small cross-correlation of the galaxy clustering data with the Planck weak lensing, which we neglect.

of the EFTofLSS in [24, 36, 37, 38, 39, 40] (see also [41]), the halo and matter power spectra and bispectra (including all cross correlations) in [24, 37]. Redshift space distortions have been developed in [25, 42, 39]. Neutrinos has been included in the EFTofLSS in [43, 44], clustering dark energy in [45, 18, 46, 47], and primordial non-Gaussianities in [37, 48, 49, 50, 42, 51]. Faster evaluation schemes for evaluation for some of the loop integrals have been developed in [52].

Main Results: The main results of our analysis are maybe best represented by Fig. 1. Using late-time measurements only, FS+BAO+SN, but with a BBN prior on the baryons abundance, we obtain a tight bound: $w = -1.046^{+0.055}_{-0.052}$ at 68% C.L. This is looser than, but nevertheless competitive with, Planck2018 [4] combined with other probes. Additionally, our limits appear to be an improvement with respect to DES results when not using CMB information [61, 62], though it is difficult to perform a precise and quantitative comparison in this case due to different combinations of external data sets and priors being used. It is hard to make a direct comparison with former BOSS analyses [63] as well, because in this case their results are presented always in combination with Planck. All products, plots, confidence intervals, results, etc., of our analyses are shown in sec. 2, and physical explanations on how all parameters from wCDM (but in fact several extensions of Λ CDM) can be measured independently using FS+BAO are discussed in sec. 3. Fitting the combination of all datasets, we obtain: $w = -1.023^{+0.033}_{-0.030}$.

Public Fast Code: Details on the code used to fit the FS, called PyBird: Python code for Biased tracers in redshift space, are given in sec. 4. In fact, an additional result of this paper is making available to the general community a fast and simple python-based code to perform the FS analysis of the power spectrum using the EFTofLSS. Pybird can be found at https://github.com/pierrexyz/pybird, where we also provide an explicit likelihood to be used in the MonteCarlo sampler MontePython [64, 65].

2 Results on wCDM

$2.1 ext{ FS} + BAO (+ SN)$

Here we present our results on the CMB-independent analysis of the wCDM model with fixed neutrino masses. The datasets we use are the following:

- FS refers to the combination of the power spectra (monopole and quadrupole) of the three different sky-cuts CMASS NGC, CMASS SGC and LOWZ NGC. These are at the effective redshift $z_{\text{eff}} = 0.57$ for CMASS and $z_{\text{eff}} = 0.32$ for LOWZ, and the maximum wavenumber we consider is $k_{\text{max}} = 0.23h/\text{Mpc}$ for CMASS and $k_{\text{max}} = 0.20h/\text{Mpc}$ for LOWZ. Ref. [1, 3] showed that in Λ CDM, with this choice of k_{max} , the theoretical systematic error is negligible for this data set with the theoretical model that we use. More explanations on this analysis are given at the beginning of appendix Λ .
- FS+BAO refers to the combination of the previous dataset with the Hr_s and D_A/r_s parameters measured from the post-reconstructed power spectra corresponding to the same sky-cuts. We include the covariance among these datasets calculated as explained in appendix A. In addition, we add 'small-z' BAO measurements at redshift $z_{\rm eff} = 0.106$ from 6DF and $z_{\rm eff} = 0.15$ from SDSS DR7 MGS, as well as Ly α BAO measurements including auto-correlation and cross-correlation with quasars from eBOSS at $z_{\rm eff} = 2.34$

FS+BAO	best-fit	$mean \pm \sigma$	FS+BAO+SN	best-fit	mean $\pm \sigma$
$w_{0,fld}$	-1.085	$-1.101^{+0.14}_{-0.11}$	$w_{0,fld}$	-1.031	$-1.046^{+0.055}_{-0.052}$
$100 \ \omega_b$	2.229	$2.236^{+0.051}_{-0.05}$	$100 \ \omega_b$	2.235	$2.235^{+0.051}_{-0.052}$
ω_{cdm}	0.122	$0.1286^{+0.009}_{-0.011}$	ω_{cdm}	0.1218	$0.1273^{+0.0088}_{-0.011}$
H_0	69.68	$70.53^{+2.4}_{-2.9}$	H_0	68.69	$69.52_{-1.7}^{+1.5}$
$\ln\left(10^{10}A_s\right)$	2.791	$2.664^{+0.22}_{-0.24}$	$\ln\left(10^{10}A_s\right)$	2.777	$2.724^{+0.19}_{-0.18}$
n_s	0.9447	$0.9071^{+0.057}_{-0.056}$	n_s	0.9273	$0.9144^{+0.055}_{-0.053}$
$\Omega_{0,fld}$	0.7014	$0.695^{+0.018}_{-0.017}$	$\Omega_{0,fld}$	0.6931	$0.6892^{+0.012}_{-0.011}$
σ_8	0.7368	$0.7062^{+0.049}_{-0.057}$	σ_8	0.7144	$0.7155^{+0.045}_{-0.051}$
FS+BAO w/o Ly-α	best-fit	$mean \pm \sigma$	$FS+BAO+SN$ w/o Ly- α	best-fit	$mean \pm \sigma$
$w_{0,fld}$	-1.021	$-1.109^{+0.17}_{-0.15}$	$w_{0,fld}$	-1.077	$-1.083^{+0.07}_{-0.056}$
$100 \ \omega_b$	2.236	$2.239^{+0.051}_{-0.051}$	$100 \omega_b$	2.247	$2.238^{+0.052}_{-0.05}$
ω_{cdm}	0.1298	$0.1439^{+0.013}_{-0.019}$	ω_{cdm}	0.1405	$0.1434^{+0.012}_{-0.019}$
77		100	**		110
H_0	69.2	$71.88^{+2.9}_{-3.7}$	H_0	71.28	$71.44^{+1.8}_{-2.5}$
$ \begin{array}{c c} H_0 \\ \ln\left(10^{10}A_s\right) \end{array} $	69.2 2.701	$ \begin{array}{c c} 71.88^{+2.9}_{-3.7} \\ 2.537^{+0.24}_{-0.27} \end{array} $	$ \begin{array}{c c} H_0 \\ \ln\left(10^{10}A_s\right) \end{array} $	71.28 2.656	$ \begin{array}{c} 71.44_{-2.5}^{+1.8} \\ 2.553_{-0.21}^{+0.2} \end{array} $
$\ln\left(10^{10}A_s\right)$	2.701	$2.537^{+0.24}_{-0.27}$	$\ln\left(10^{10}A_s\right)$	2.656	$2.553^{+0.2}_{-0.21}$

Table 1: Results on wCDM fitting various combinations of FS with BAO and SN.

and $z_{\text{eff}} = 2.35$ respectively, based on the likelihood of [66]. All these redshift bins are uncorrelated with the redshift bins of FS+BAO.

• FS+BAO+SN refers to the combination of the previous dataset plus the Pantheon catalogue of high-redshift supernovae.

We use a Gaussian prior on ω_b motivated from BBN constraints centered on 0.02235 with $\sigma_{\rm BBN} = 0.0005$, which is obtained by adding up the theory and statistic error of [67]. The fit is done considering the Planck prescription of one single massive neutrino with mass 0.06 eV as done in [4]. The best fits, means and one-sigma intervals of the 1D posteriors are given in Table 1. The triangle plots are shown in Fig. 2, while the $w - \Omega_m$ contour is shown in Fig. 1. Following [1], we compare our analysis pipeline with simulations in App. A, finding negligible theoretical systematic errors in wCDM.

For our constraints on wCDM, we only show the results for FS + BAO and FS + BAO + SN, since the FS dataset alone does not constrain w very well, as this is subject to strong degeneracies. This is to be expected, as we analyze only two close redshift bins with $z_{\rm eff} = 0.32$ and $z_{\rm eff} = 0.57$. When adding BAO, w is constrained to $w = -1.101 \pm 0.12$ at 68% C.L. (± 0.25 at 95% C.L.). Much of the improvement is coming from the addition of the small-z bins with $z_{\rm eff} = 0.106$ from 6DF and $z_{\rm eff} = 0.15$ from SDSS DR7 MGS at which dark energy has strong effect on the background evolution, allowing to further break the degeneracies. Adding Ly- α BAO breaks even more the degeneracies, as it adds one more redshift point deep into matter domination. These combinations of FS plus the various BAO are shown in Fig. 4, and more discussions can be found in sec. 3.

Although the result from FS+BAO does not set a very strong constraint on w, it is

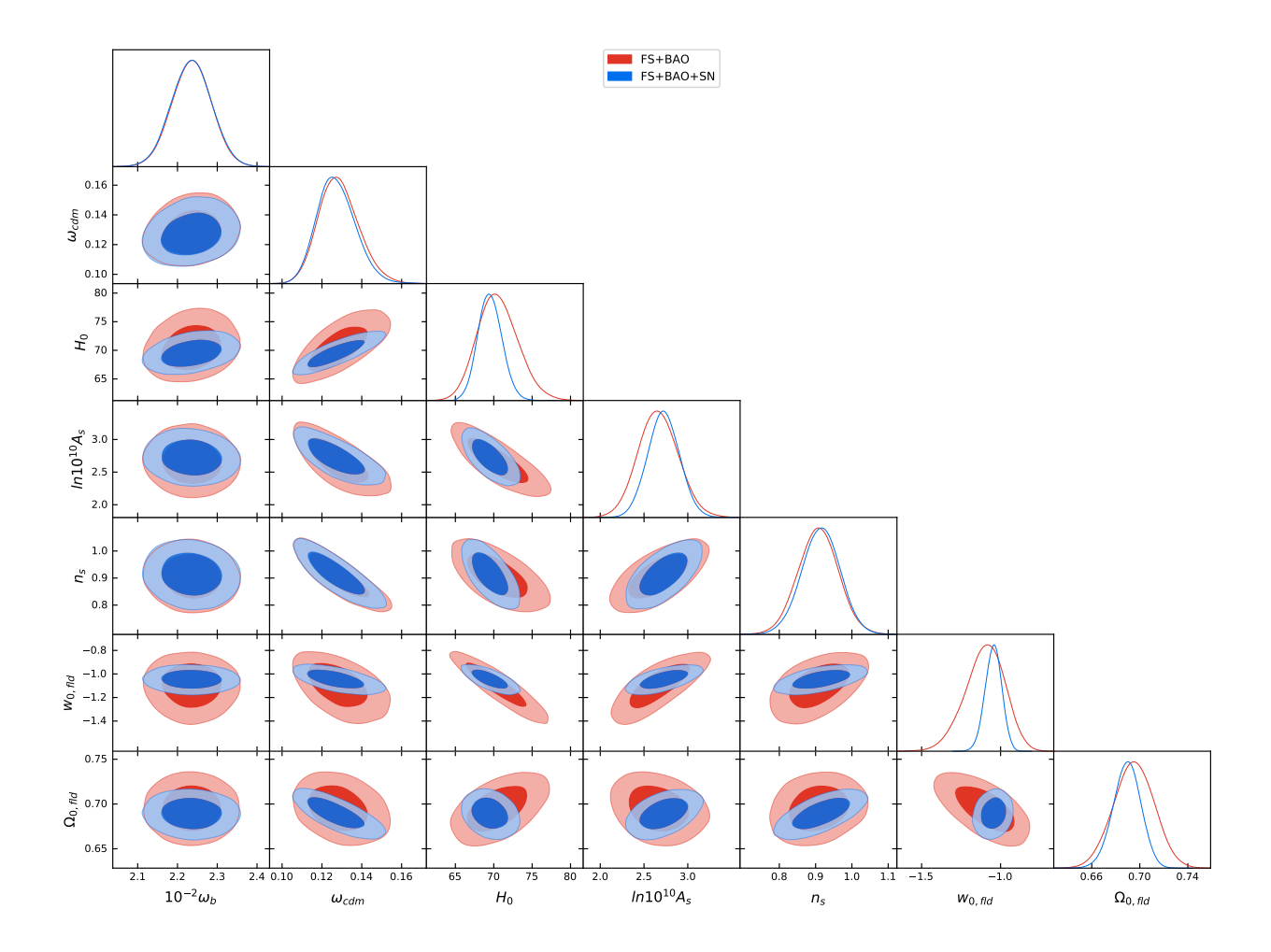


Figure 2: Triangle plot of wCDM fitting various combinations of FS with BAO and SN.

interesting in itself since it shows the ability to measure dark energy evolution using only late-time observables. Notice that the limits on w from the BOSS (+SDSS/6DF) data are stronger than the ones from Planck2018 (+ lensing) alone, which measures w to $-1.57^{+0.16}_{-0.33}$ at 68% C.L. ($^{+0.50}_{-0.40}$ at 95% C.L.) [4].

The ability to measure w with FS+BAO is to be contrasted with the SN measurements, which require an external input (usually from the CMB) to achieve competitive precision, to break the degeneracy line in the plane $w - \Omega_m$. The SN constraint on $w - \Omega_m$ comes from the fact that they provide a measurement of the luminosity distance $D_L(z)$. We can estimate the scaling on parameters at the median redshift of the SN sample, getting $D_L(z = 0.25) \sim \Omega_m^{-0.055} |w|^{0.1}$, as can be inferred from table. 3. This is to be contrasted with the positive correlation between w and Ω_m given by the FS+BAO measurements, as discussed in sec. 3. Therefore, the combination FS+BAO+SN allows a much tighter constraint on $w = -1.046^{+0.055}_{-0.052}$. This sets a competitive limit from late-time measurements alone, and it is consistent with previous analyses.

For instance, combined Planck2018 and BAO gives $w = -1.038^{+0.055}_{-0.048}$ [4], while combined Planck2015 and SN yields $w = -1.026 \pm 0.041$ [55]. This strongly suggests that additional

CMB+BAO	best-fit	mean $\pm \sigma$	CMB+FS	best-fit	mean $\pm \sigma$
$w_{0,fld}$	-1.035	$-1.045^{+0.056}_{-0.051}$	$w_{0,fld}$	-1.027	$-1.029^{+0.063}_{-0.056}$
$100 \ \omega_b$	2.24	$2.238^{+0.014}_{-0.014}$	$100 \ \omega_b$	2.241	$2.238^{+0.014}_{-0.014}$
ω_{cdm}	0.12	$0.12^{+0.0011}_{-0.0011}$	ω_{cdm}	0.1199	$0.12^{+0.0011}_{-0.0011}$
$100 * \theta_s$	1.042	$1.042^{+0.0003}_{-0.00029}$	$100 * \theta_s$	1.042	$1.042^{+0.00029}_{-0.00028}$
$\ln\left(10^{10}A_s\right)$	3.051	$3.047^{+0.014}_{-0.015}$	$\ln\left(10^{10}A_s\right)$	3.047	$3.044^{+0.014}_{-0.015}$
n_s	0.9667	$0.9658^{+0.0039}_{-0.0041}$	n_s	0.9648	$0.9656^{+0.004}_{-0.004}$
$ au_{reio}$	0.05767	$0.05514^{+0.0073}_{-0.0078}$	$ au_{reio}$	0.05567	$0.05385^{+0.0073}_{-0.0077}$
z_{reio}	8.021	$7.751_{-0.76}^{+0.76}$	z_{reio}	7.817	$7.623^{+0.77}_{-0.75}$
$\Omega_{0,fld}$	0.6951	$0.697^{+0.012}_{-0.012}$	$\Omega_{0,fld}$	0.6935	$0.6923^{+0.016}_{-0.016}$
YHe	0.2479	$0.2478^{+6.1e-05}_{-6.1e-05}$	YHe	0.2479	$0.2478^{+6.1e-05}_{-6.1e-05}$
H_0	68.49	$68.75^{+1.3}_{-1.5}$	H_0	68.3	$68.26^{+1.6}_{-1.8}$
σ_8	0.8239	$0.8244^{+0.016}_{-0.017}$	σ_8	0.819	$0.8189^{+0.016}_{-0.018}$
CMB+FS+BAO	best-fit	$mean \pm \sigma$	CMB+FS+BAO+SN	best-fit	$mean\pm\sigma$
$w_{0,fld}$	-1.018	$-1.021^{+0.049}_{-0.044}$	$w_{0,fld}$	-1.028	$-1.023^{+0.033}_{-0.03}$
$100 \ \omega_b$	2.238	$2.24^{+0.014}_{-0.014}$	$100 \omega_b$	2.236	$2.24^{+0.014}_{-0.014}$
ω_{cdm}	0.1198	$0.1197^{+0.0011}_{-0.0011}$	ω_{cdm}	0.1202	$0.1197^{+0.0011}_{-0.001}$
$100 * \theta_s$	1.042	$1.042^{+0.00029}_{-0.00029}$	$100 * \theta_s$	1.042	$1.042^{+0.00029}_{-0.00029}$
$\ln\left(10^{10}A_s\right)$	3.038	$3.045^{+0.014}_{-0.015}$	$\ln\left(10^{10}A_s\right)$	3.036	$3.045^{+0.014}_{-0.015}$
n_s	0.9654	$0.9664^{+0.004}_{-0.0039}$	n_s	0.9658	$0.9663^{+0.0039}_{-0.004}$
$ au_{reio}$	0.0526	$0.05492^{+0.0072}_{-0.0077}$	$ au_{reio}$	0.0507	$0.05464^{+0.0072}_{-0.0076}$
z_{reio}	7.509	$7.722^{+0.76}_{-0.74}$	z_{reio}	7.321	$7.694^{+0.76}_{-0.73}$
$\Omega_{0,fld}$	0.6909	$0.6926^{+0.012}_{-0.011}$	$\Omega_{0,fld}$	0.6914	$0.6931^{+0.008}_{-0.0078}$
YHe	0.2478	$0.2479^{+5.9e-05}_{-6e-05}$	YHe	0.2478	0.2479^{+6e-05}_{-6e-05}
H_0	67.98	$68.18^{+1.2}_{-1.3}$	H_0	68.13	$68.22^{+0.82}_{-0.86}$
σ_8	0.8126	$0.8162^{+0.014}_{-0.015}$	σ_8	0.8161	$0.8168^{+0.011}_{-0.011}$

Table 2: Results on wCDM fitting different combinations of CBM with FS, BAO and SN.

data from future spectroscopic and photometric surveys will allow to constrain dark energy in an unprecedented way.

2.2 Combined CMB and FS + BAO (+ SN)

In order to get the tightest constraints possible on $w - \Omega_m$, we add the Planck2018 datasets to the FS, BAO and SN. When adding Planck2018, we include the temperature, polarization and lensing likelihoods as provided by the Planck collaboration, that we will refer as 'CMB'. As for the nuisance parameters, we only consider the 'lite' configuration with one nuisance parameter, since we verified that it gives very similar results with respect to the full configuration. When combined to CMB, we do not include Lyman- α BAO to faciliate comparison with other analyses. We checked that including them does not change the results. The best-fits, means and one-sigma intervals of the 1D posteriors are given in Table 2. The triangle plots are shown in Fig. 3, and the $w - \Omega_m$ contour is shown in Fig. 1.

The results we get on CMB + BAO are similar to the one of [4]. Our CMB + BAO constraint is $w = -1.045^{+0.056}_{-0.051}$, while CMB + FS gives $w = -1.029^{+0.063}_{-0.056}$, a similar constraint

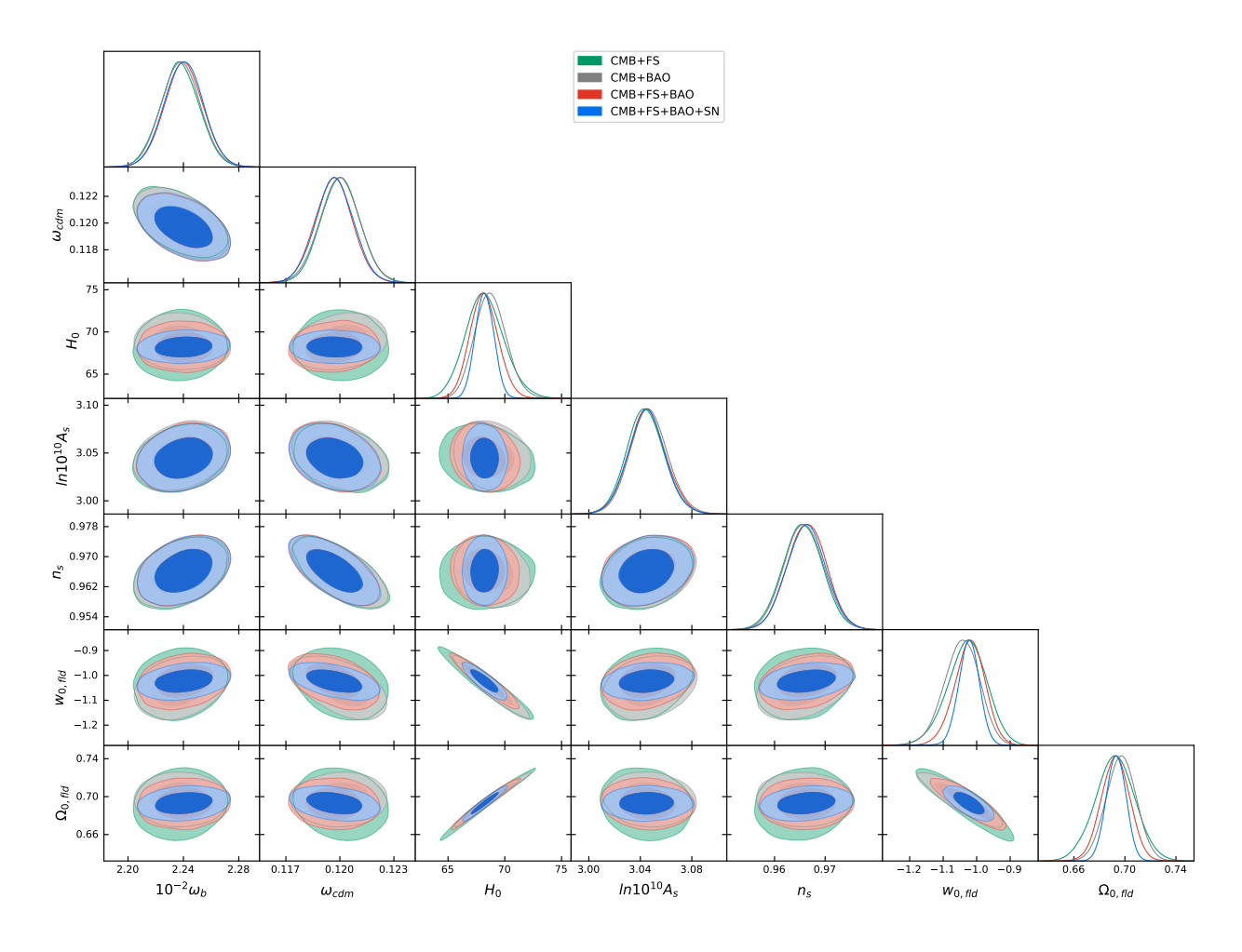


Figure 3: Triangle plot of wCDM fitting various combinations of CMB with FS, BAO and SN.

with a slight shift towards -1. As argued in [68] for the Λ CDM model, the similar error bars for the CMB + BAO and CMB + FS analyses are a coincidence given the BOSS volume and the reconstruction algorithm used to measure the BAO parameters: it is expected that the FS information will supersede the BAO information in the next-generation experiments. At this stage, we note that both the FS and the BAO information break the degeneracy in the $w - \Omega_m$ plane displayed by the Planck fit alone. The combination of CMB + FS + BAO gives an even tighter constraint: $w = -1.021^{+0.049}_{-0.044}$, which is about a 15% improvement on the error bar compared to CMB + BAO. This shows that the FS does add information on top of the BAO, even when in combination with CMB. Finally, adding SN provides $w = -1.021^{+0.033}_{-0.030}$, our tightest constraint. This combination gives similar error bars as CMB+BAO+SN measurements, $w = -1.028 \pm 0.031$ [4], but a slight shift towards -1.

3 Physical Considerations

Let us now try to understand analytically how the data allow us to break the degeneracies and give constraints on w, following the discussion in [1], which, in turns, is similar to what done for the CMB in [69].

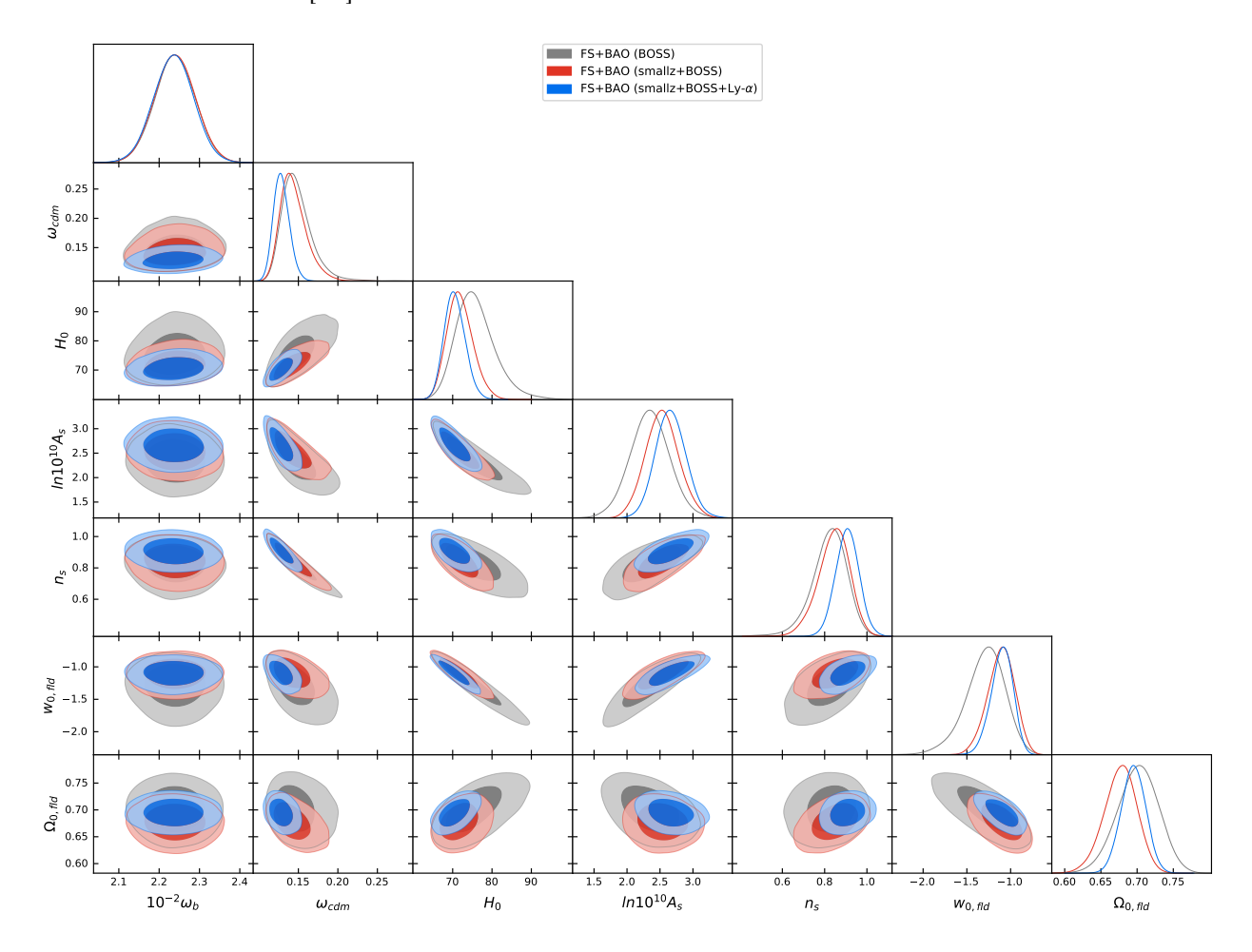


Figure 4: Triangle plot of wCDM fitting the FS in combination with various BAO: BOSS, BOSS+small-z (SDSS DR7 MGS/6DF) and BOSS+small-z+Lyman- α .

First, we notice that changing w does not impact the shape of the primordial power spectrum. The only effects are the modifications of the linear growth function and of the angular diameter distance, which affects the angular scale under which the BAO peak is seen.

BAOs mainly measure the combination $\theta_{LSS,V} = \left(\theta_{LSS,\perp}^2 \theta_{LSS,\parallel}\right)^{\frac{1}{3}}$, where $\theta_{LSS,\perp}$ and $\theta_{LSS,\parallel}$ are the contributions perpendicular and parallel to the line of sight, which can be disentangled from measuring separately the monopole and the quadrupole of the power spectrum in the FS analysis, or from measuring the anisotropic BAO parameters. The angles are the following ratios of length scales:

$$\theta_{\rm LSS,\perp} \simeq \frac{r_d(z_{\rm CMB})}{D_A(z_{\rm LSS})}, \quad \theta_{\rm LSS,\parallel} \simeq \frac{r_d(z_{\rm CMB})}{c z_{\rm LSS}/H(z_{\rm LSS})},$$
 (1)

	$ heta_{\mathrm{LSS},\perp}$			$ heta_{ m LSS,\parallel}$			$ heta_{ m LSS,V}$	
	$z_{ m CMASS}$	$z_{ m LOWZ}$	$z_{\mathrm{Ly}-lpha}$	$z_{ m CMASS}$	$z_{ m LOWZ}$	$z_{{ m Ly}-lpha}$	$z_{ m 6dF}$	$z_{ m MGS}$
ω_m	-0.14	-0.19	0.15	-0.027	-0.12	0.20	-0.23	-0.21
h	0.77	0.86	0.45	0.54	0.72	0.84	0.94	0.91
w	-0.17	-0.12	-0.19	-0.25	-0.21	-0.11	-0.065	-0.087

	L)	f	D_L	
	$z_{ m CMASS}$ $z_{ m LOWZ}$		$z_{ m CMASS}$	$z_{ m LOWZ}$	z = 0.25
ω_m	-0.12	-0.08	0.30	0.40	-0.055
h	0.25	0.16	-0.59	-0.80	-0.89
w	-0.063	-0.028	0.29	0.25	0.10

Table 3: Logarithmic derivatives of different observables with respect to cosmological parameters.

where $r_d(z_{\text{CMB}})$ is the sound horizon at drag redshift, and z_{LSS} is the mean redshift of the data sample. Following [1], to understand the approximate parameter scaling, we take the log derivatives around a fiducial cosmology ($\omega_m = 0.147$, h = 0.7, w = -1), shown in tab. 3 for several quantities of interest.

From the table, we can read the approximate degeneracy lines for CMASS, LOWZ, small-z and $\text{Ly}\alpha$:

$$\theta_{\text{LSS},\perp}(z_{\text{CMASS}}) \sim \left(h\,\omega_m^{-0.18}|w|^{-0.22}\right)^{0.77}, \qquad \theta_{\text{LSS},\parallel}(z_{\text{CMASS}}) \sim \left(h\,\omega_m^{-0.05}|w|^{-0.47}\right)^{0.54}, \theta_{\text{LSS},\perp}(z_{\text{LOWZ}}) \sim \left(h\,\omega_m^{-0.22}|w|^{-0.14}\right)^{0.86}, \qquad \theta_{\text{LSS},\parallel}(z_{\text{LOWZ}}) \sim \left(h\,\omega_m^{-0.16}|w|^{-0.29}\right)^{0.72}, \theta_{\text{LSS},V}(z_{\text{6dF}}) \sim \left(h\,\omega_m^{-0.25}|w|^{-0.069}\right)^{0.94}, \qquad \theta_{\text{LSS},V}(z_{\text{MGS}}) \sim \left(h\,\omega_m^{-0.23}|w|^{-0.096}\right)^{0.91}, \theta_{\text{LSS},\parallel}(z_{\text{Ly}\alpha}) \sim \left(h\,\omega_m^{2.4}|w|^{-1.3}\right)^{0.84}, \qquad \theta_{\text{LSS},\perp}(z_{\text{Ly}\alpha}) \sim \left(h\,\omega_m^{0.33}|w|^{-0.42}\right)^{0.45}.$$
(2)

The relative amplitude of the BAO wiggles with respect to the smooth part instead gives a measurement of $\sim \omega_m$. This is quite intuitive as, unlike the wavelength, the amplitude of the oscillating part is not affected by projection effects, and therefore simply scales as the density of baryons and dark matter at the time of recombination, which, in the case of fixed ω_b , simply scales as ω_m (see [70] for a very pedagogical review and derivation).

Let us now consider the broad-band signal. The linear power spectrum monopole and quadrupole give a measurement of $b_1^2 A_s^{(k_{\text{max}})}$ and $b_1 f A_s^{(k_{\text{max}})}$, where $f(z_{\text{CMASS}}) \sim \Omega_m^{0.3} |w|^{0.29}$ and $f(z_{\text{LOWZ}}) \sim \Omega_m^{0.4} |w|^{0.25}$, f being the log-derivative of the linear growth function. Here $A_s^{(k_{\text{max}})}$ represents the amplitude of the linearly evolved power spectrum at the maximum wavenumber of our analysis, as this is where the signal peaks. The broadband signal gives also a measurement of the linear growth function D since the linear power spectrum scales as D^2 , while the loop one scales as D^4 . However, the dependence on w is quite weak, since $D(z_{\text{CMASS}}) \sim \Omega_m^{-0.12} |w|^{-0.063}$ and $D(z_{\text{LOWZ}}) \sim \Omega_m^{-0.08} |w|^{-0.028}$.

These estimates allow us, in principle, to solve for the cosmological parameters of the wCDM model when using only LSS data. We determine ω_m from the amplitude of the BAO oscillations. Then, the BAO angles, the quadrupole/monopole ratio and the amplitude of the broadband signal will give a measurement of h, A_s and w (as well as of b_1). However,

using only the FS dataset there will be large error bars in the recovered parameters, given the low precision of the quadrupole spectra, and of the LOWZ measurements. In particular, we find a large anticorrelation among w and h, and a positive correlation between w and A_s , as predicted by our simple analysis 3 .

When adding the precise BAO data from the post-reconstructed power spectra, we are able to partially break the degeneracies. A big improvement comes from adding small-z BAO measurements, as we have additional data points to break the h-w degeneracy (and the $w-A_s$ one as a consequence), getting the final constraints in fig. 4. The shift in the posteriors when adding small-z BAO is consistent with what we observe in our tests on simulations, see App. A.

When we add SN data, we get a measurement of the luminosity distance $D_L = (1+z)^2 D_A$. In the absence of calibration of absolute luminosities, we cannot determine h and one gets the approximate degeneracy line $D_L(z=0.25) \sim \Omega_m^{-0.055} |w|^{0.1}$. This is an anticorrelation between Ω_m and w, apparent from fig. 1. As we discussed, FS+BAO data give an anticorrelation between h and w since ω_m is determined. Therefore, w and $\Omega_m \sim \omega_m/h^2$ are positively correlated. This explains the good constraints we get when we add the SN dataset to FS+BAO.

4 PyBird: Python code for Biased tracers in redshift space

PyBird is a code written in Python 3, designed for evaluating the multipoles of the power spectrum of biased tracers in redshift space. In general, PyBird can evaluate the power spectrum of matter or biased tracers in real or redshift space. The equations on which PyBird is based can be found in [39, 1]. The main technology used by the code is the FFTLog [71] ⁴, used to evaluate the one-loop power spectrum and the IR resummation, see sec. 4.1 for details.

PyBird is designed for a fast evaluation of the power spectra, and can be easily inserted in a data analysis pipeline. In fact, it is a standalone tool whose input is the linear matter power spectrum which can be obtained from any Boltzmann code, such as CAMB [72] or CLASS [73]. The Pybird output can be used in a likelihood code which can be part of the routine of a standard MCMC sampler.

The code is public and available at: https://github.com/pierrexyz/pybird, and it depends on the numerical libraries NumPy [74] and SciPy [75]. We also provide an explicit integration in the MCMC sampler MontePython 3 [64], as well as a Jupyter notebook containing examples to start with.

The design is modular and concise, such that parts of the code can be easily adapted to other case uses (e.g., power spectrum at two loops or bispectrum). PyBird consists of the

 $^{^{3}}$ To understand the sign of the correlation, notice that w is negative, and so to make it larger in absolute value, it will move towards more negative values.

⁴https://jila.colorado.edu/ajsh/FFTLog/index.html

following classes:

- Bird: Main class which contains the power spectrum and correlation function, given a cosmology and a set of EFT parameters.
- Nonlinear: given a Bird() object, computes the one-loop power spectrum and one-loop correlation function.
- Resum: given a Bird() object, performs the IR-resummation of the power spectrum.
- Projection: given a Bird() object, applies geometrical effects on the power spectrum: Alcock-Paczynski effect, window functions, fiber collisions, binning.
- Common: containing shared objects among the other classes, such as k-array, multipole decomposition, etc.

PyBird can be used in different ways. The code can evaluate the power spectrum either given one set of EFT parameters, or independently of the EFT parameters. If the former option is faster, the latter is useful for subsampling or partial marginalization over the EFT parameters, or to Taylor expand around a fiducial cosmology for efficient parameter exploration [3]. PyBird runs in less than a second on a laptop.

We performed extensive tests on PyBird numerics, with particular attention on the numerical stability of the FFTLog. Especially, zero padding and window are implemented following [76]. All numerical parameters (e.g. number of points, boundaries or bias of the FFTLog's) are chosen such as, for a given value, we get the same power spectrum for that value multiplied or divided by 2, within 0.02% for l=0, and 0.2% for l=2, up to $k\sim 0.3$. In the same spirit, the Taylor expansions in the IR-resummation are under control.

Notice finally that the particular implementation of the IR-resummation that we describe next allows for a simple modification of the code so that the dependence on A_s can be factorized. Therefore, the sampling over A_s could be done extremely fast.

4.1 Fast IR-resummation scheme

The resummed power spectrum can be written as a sum of the nonresummed power spectrum plus IR-corrections. These IR-corrections can be efficiently evaluated using the FFTLog, which allows for a quick evaluation. In this appendix, we derive the mathematical details of such implementation.

After a straightforward manipulations, the IR-resummation in redshift space for biased tracers up to the N-loop order reads [25, 42]:

$$P^{\ell}(k)|_{N} = \sum_{j=0}^{N} \sum_{\ell'} 4\pi (-i)^{\ell'} \int dq \, q^{2} \, Q_{||N-j}^{\ell\ell'}(k,q) \, \xi_{j}^{\ell'}(q), \tag{3}$$

$$\xi_j^{\ell'}(q) = i^{\ell'} \int \frac{dp \, p^2}{2\pi^2} P_j^{\ell'}(p) \, j_{\ell'}(pq). \tag{4}$$

where $|_N$ denotes the resummed power spectrum up to order N and $P_j^{\ell}(k)$ and $\xi_j^{\ell}(k)$ are the j-loop order piece of the Eulerian power spectrum and correlation function, respectively. $Q_{||N-j}^{\ell\ell'}(k,q)$ encodes the effects from the bulk displacements and is given by:

$$Q_{||N-j|}^{\ell\ell'}(k,q) = \frac{2\ell+1}{2} \int_{-1}^{1} d\mu_k \, \frac{i^{\ell'}}{4\pi} \int d^2\hat{q} \, e^{-i\boldsymbol{q}\cdot\boldsymbol{k}} \, F||_{N-j}(\boldsymbol{k},\boldsymbol{q}) \mathcal{P}_{\ell}(\mu_k) \mathcal{P}_{\ell'}(\mu_q), \tag{5}$$

 $F|_{N-j}(\mathbf{k}, \mathbf{q}) = T_{0,r}(\mathbf{k}, \mathbf{q}) \times T_{0,r}^{-1}|_{N-j}(\mathbf{k}, \mathbf{q}),$

$$T_{0,r}(\mathbf{k},\mathbf{q}) = \exp\left\{-\frac{k^2}{3}\left[\Xi_0(q)(1+2f\mu_k^2+f^2\mu_k^2) + \Xi_2(q)\left((\hat{k}\cdot\hat{q})^2 + 2f\mu_k\mu_q(\hat{k}\cdot\hat{q}) + f^2\mu_k^2\mu_q^2\right)\right]\right\},\,$$

where $\Xi_0(q)$ and $\Xi_2(q)$ are given by:

$$\Xi_0(q) = \int \frac{dp}{2\pi^2} \exp\left(-\frac{p^2}{\Lambda_{\rm IR}^2}\right) P_{11}(p) \left[1 - j_0(pq)\right], \tag{6}$$

$$\Xi_2(q) = \int \frac{dp}{2\pi^2} \exp\left(-\frac{p^2}{\Lambda_{\rm IR}^2}\right) P_{11}(p) j_2(pq).$$
 (7)

By expanding the exponential in $F|_{N-j}(\mathbf{k}, \mathbf{q})$ in powers of k^2 and performing the angular integrals in Eq. (5) ⁵, the terms in Eq. (3) can be put in the form of:

$$4\pi(-i)^{\ell'}k^{2n}\,\mathcal{Q}_{||N-j}^{\ell\ell'}(n,\alpha)\,\int dq\,q^2\,\left[\Xi_i(q)\right]^n\xi_j^{\ell'}(q)\,j_\alpha(kq),\tag{8}$$

where n is the integer power controlling the expansion of the exponential, j_{α} is the α -th order spherical Bessel function, $[\Xi_{i}(q)]^{n}$ denotes a product of the form $\Xi_{0}(q) \times ... \times \Xi_{0}(q) \times \Xi_{2}(q) \times ... \times \Xi_{2}(q)$ such that the total number of terms in the product is n, and $\mathcal{Q}_{||N-j}^{\ell\ell'}(n,\alpha)$ is a number that depends on N-j, ℓ , ℓ' , n, α (and f). In particular, at lowest order n=0, one gets nothing but the nonresummed power spectrum. The contributions to the integrand of Eq. (8) are shown in Fig. 5.

Thus, the resummed power spectrum is equal to the nonresummed power spectrum plus IR-corrections written as an expansion in powers of k^2 (starting at k^2):

$$P^{\ell}(k)|_{N} = P^{\ell}(k) + \sum_{j=0}^{N} \sum_{\ell'} \sum_{n=1} \sum_{\alpha} 4\pi (-i)^{\ell'} k^{2n} \mathcal{Q}_{||N-j|}^{\ell\ell'}(n,\alpha) \int dq \, q^{2} \left[\Xi_{i}(q)\right]^{n} \xi_{j}^{\ell'}(q) \, j_{\alpha}(kq) \,, \tag{9}$$

where we remind that n is the integer controlling the expansion in powers of k^2 of the exponential of the bulk displacements, running up to a sufficient order to achieve convergence of the expansion up to the highest k mode of interest. The explicit expressions for $\mathcal{Q}_{||N-j}^{\ell\ell'}(n,\alpha)$ can be found in PyBird repo either in the main code or in the Mathematica notebook. Therefore, evaluating the resummed power spectrum boils down to evaluating one-dimensional integrals that can be performed using the FFTLog. The loops of the (nonresummed) power spectrum and correlation function can be evaluated using the FFTLog, see e.g. [52, 28]. Then,

⁵To perform the angular integrals, we follow the steps of [42], but here expanding the whole argument of the exponential.

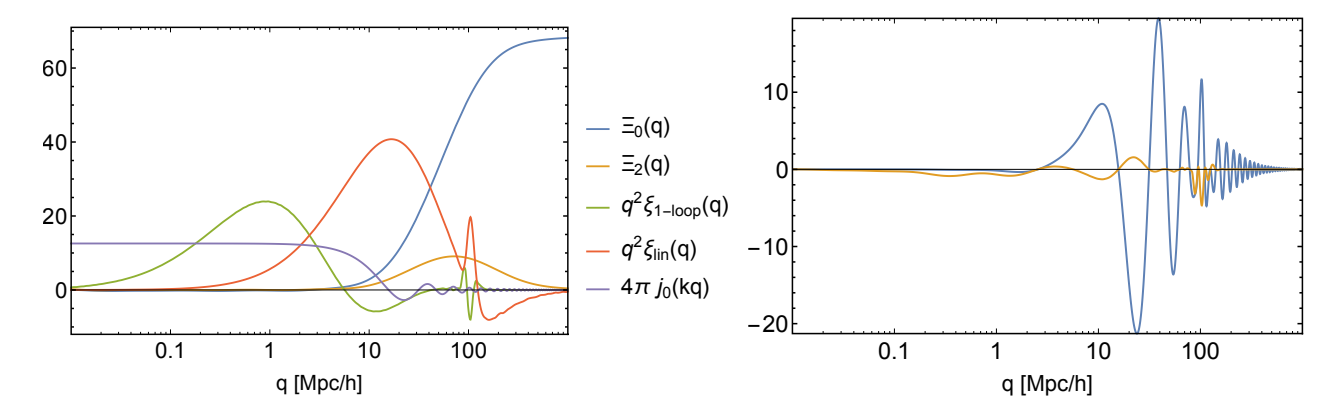


Figure 5: Left: Various contributions appearing in the leading IR-corrections, Eq. (8) with n=1, for the matter real-space power spectrum, with k=0.2. $\Xi_0(q)$ or $\Xi_2(q)$ are essentially acting as lowcut and a bandpass filters around the BAO peak, respectively, making the BAO the only relevant information for the IR-resummation, while the broadband is mostly filtered out. This illustrates the physical fact that the IR-resummation only acts on the wiggly part of the power spectrum. Right: Typical IR-correction integrand for the linear part (blue) and the one-loop (orange), at k=0.2, of the form: $4\pi q^2 \xi_j(q) \left[e^{-\frac{k^2}{3}\Xi_0(q)}-1\right] j_0(kq)$. While the broadband information is irrelevant, most of the signal in the integral will come from the BAO.

the IR-resummation consists simply in correcting the power spectrum with a set of spherical Bessel transforms that, once again, can be performed using the FFTLog. In practice, we find that expanding up to n=8 is sufficient to achieve convergence up to $k \sim 0.3h\,\mathrm{Mpc}^{-1}$ for both $\ell=0,2$, and keeping terms contributing only significantly⁶, the IR-resummation can be achieved with about 30 FFTLog's. Notice that the spherical Bessel transforms in Eq. 9 all present well-localized compact integrands around the BAO scales, allowing to perform the FFTLog with a few points ($\sim \mathcal{O}(200)$) to achieve good accuracy.

Finally, as discussed in [25, 42], the dependence on the displacements is analytic, and therefore the IR-resummation will agree to perturbation theory once this one is performed to extremely high order. In practice, indeed, in our procedure we are Taylor expanding the IR-resummation, which is equivalent to including the part of the perturbative loop that would encode the effect of the long displacements. The fact that we go to order n = 8 means that effectively we are doing an eight-loop calculation, but effectively keeping track only of the part that is relevant for the IR-resummation.

⁶Precisely, we keep only the terms with one power in $k^2\Xi_2(q)$ (see [42] for the validity of such approximation), and drop a few more terms that are found to be irrelevant.

Acknowledgements

We thank Florian Beutler and Héctor Gil-Marín for support with the BOSS data, and Emanuele Castorina for useful discussions. LS and GDA are partially supported by Simons Foundation Origins of the Universe program (Modern Inflationary Cosmology collaboration) and LS by NSF award 1720397. GDA and PZ thank the Theoretical Physics Group at CERN for hospitality during part of this work. PZ thanks Françoise Papa for hospitality during completion of this work. The linear power spectra were computed with the CLASS Boltzmann code [77] ⁷. The posteriors were sampled using MontePython cosmological parameter inference code [64, 65] ⁸. Part of the analysis was performed on the Sherlock cluster at the Stanford University, for which we thank the support team, and part on the HPC (High Performance Computing) facility of the University of Parma, whose support team we thank.

A FS + BAO joint analysis

The post-reconstructed power spectrum contains additional information in the BAO with respect to the pre-reconstructed one, by adding displacements from higher (pre-reconstructed) n-point functions. Here we describe how we analyse the BOSS DR12 pre- and post-reconstructed power spectrum.

The full shape (FS) of the pre-reconstructed power spectrum is fit with a cosmology- and survey-dependent theoretical model. For all analyses presented in this work, we fit the FS using the EFTofLSS galaxy power spectrum with IR-resummation, Alcock-Paczynski effect, window function 9 , correction for fiber collisions, and priors as described in [1] 10 . Note that when analyzing extension to the concordance model such as wCDM, the growth rate f and the relations implied in the Alcock-Paczynski effect — through H(z) and $D_A(z)$ — are modified accordingly. Note that this analysis is very similar operationally to the analyses that are normally carried out for the CMB, *i.e.* all the data points are fit with a theoretical model that is updated at every cosmology (CMB style). Meanwhile, we follow the standard treatment with fixed template but varying BAO parameters for the post-reconstructed power spectrum, see e.g. [54, 79].

When combining FS and BAO, there will be a sizeable covariance between the BAO parameters and the pre-reconstructed power spectra, which we measure from 2048 patchy mocks as follows. For the full shape part, we estimate the covariance from the Patchy pre-reconstructed power spectrum measurements. For the BAO parameters, $H(z) r_s$ and $D_A(z)/r_s$, we determine the 2048 bestfit points from the Patchy post-reconstructed power spectrum measure-

⁷ http://class-code.net

⁸ https://github.com/brinckmann/montepython public

⁹The window function has been remeasured using the technique of [78]. We thank Florian Beutler for providing them to us in [1, 3].

¹⁰With a small exception: we now put a Gaussian prior of 2 (centered on 0) on the constant stochastic term, $c_{\epsilon,1}/\bar{n}_g$, where \bar{n}_g is the mean galaxy density. This has minor consequences, as we checked that dividing or multiplying the prior by 2 barely change the results.

FS	best-fit	mean $\pm \sigma$	truth	FS+BAO	best-fit	mean $\pm \sigma$	truth
ω_{cdm}	0.1231	$0.124^{+0.0064}_{-0.0064}$	0.119	ω_{cdm}	0.1179	$0.1205^{+0.0063}_{-0.0062}$	0.119
h	0.6816	$0.682^{+0.008}_{-0.0079}$	0.6777	h	0.6744	$0.6763^{+0.0067}_{-0.0068}$	0.6777
$\ln \left(10^{10} A_s \right)$	2.95	$2.963^{+0.076}_{-0.096}$	3.091	$\ln \left(10^{10} A_s \right)$	3.057	$3.01^{+0.084}_{-0.11}$	3.091
n_s	0.9377	$0.9181^{+0.035}_{-0.035}$	0.96	n_s	0.9205	$0.9236^{+0.033}_{-0.034}$	0.96

Table 4: Results on Λ CDM fitting the mean of 2048 patchy CMASS NGC mocks FS or FS + BAO, using a covariance rescaled by 16 and a BBN prior on ω_b .

ments. The joint covariance is then estimated, together with the cross-correlation between the pre-reconstructed Patchy power spectra and the BAO parameters.

The FS analysis has been already extensively checked against simulations in [1, 3]: the theory-systematic error is under control at less than $\sigma_{\rm stat}/4$, where $\sigma_{\rm stat}$ is the statistical error obtained by fitting the BOSS DR12 pre-reconstructed power spectra up to $k_{\rm max} \sim 0.2 h\,{\rm Mpc}^{-1}$. For the joint FS+BAO analysis, we perform the following tests:

Test against simulations In Fig. 6 and Table 4, we show the marginalized posterior distribution of the Λ CDM parameters with a BBN prior on ω_b , obtained by fitting the mean over 2048 CMASS NGC Patchy mocks, analyzed with the covariance divided by 16, as done in the tests performed in [1, 3]. This rescaling allows us to measure the theory-systematic error within about $1/3 \sigma_{\text{stat}}$ of the individual 1D posteriors, where σ_{stat} is the 68% confidence interval obtained by fitting BOSS data. By measuring the theory-systematic error on simulations as the distance of the 68% confidence interval of the 1D posterior to the Patchy true value, we find no theory-systematic error except a tiny one on n_s of less than 0.01 for both FS and FS+BAO, and on $\ln(10^{10}A_s)$ of at most $1/4 \sigma_{\text{stat}}$ for FS and less for FS+BAO, thus safely negligible. Importantly, adding BAO moves very little the mean of the posteriors: the shifts are at most $1/4 \sigma_{\text{stat}}$. This is already safe when analyzing BOSS data alone, and the systematic error becomes completely negligible when combined with the Planck2018 likelihood. Notice also that adding BAO moves the posteriors towards the true cosmology of the simulation.

Fit to BOSS data We fit the BOSS data with a $\nu\Lambda$ CDM model with 3 massive neutrinos obeying a normal hierarchy with a flat prior on the total mass: $0.06 \leq \sum_i m_{\nu,i}/\text{eV} \leq 1.0$ and a BBN prior on ω_b . The results are shown in Fig. 7 and in Table 5. We find no shift in the cosmological parameters when adding BAO except on H_0 , for which the shift is less that $1/4 \sigma_{\text{stat}}$.

Covariance Given that the pre-reconstruction and the post-reconstruction data set are quite correlated, it is important to accurately measure the cross correlation in order to ensure potential cancellations. We compare the covariance measured from 2048 patchy mocks against another covariance measured from 1024 Patchy mocks. We find the same amount of correlation between the BAO parameters, as well as between them and the individual k-bins of the FS. We analyze the Patchy mocks as in Fig. 6 but with the covariance measured with

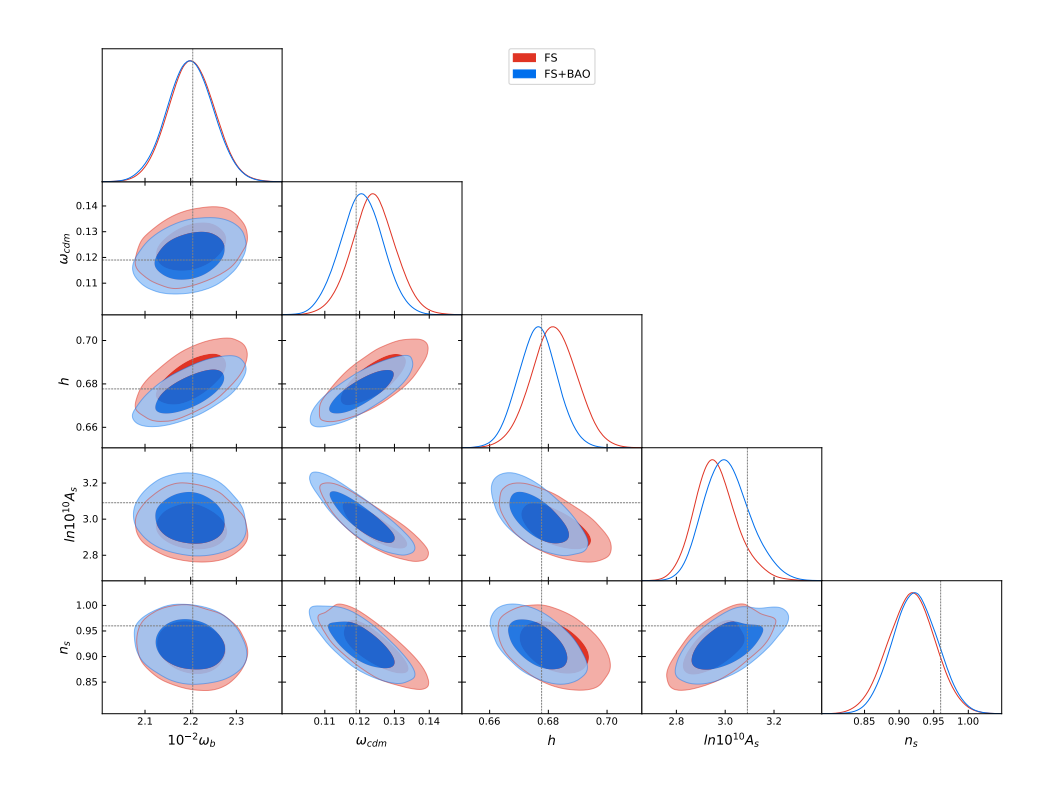


Figure 6: Triangle plot of Λ CDM fitting the mean of 2048 patchy CMASS NGC mocks FS or FS + BAO, using a covariance rescaled by 16 and a BBN prior on ω_b .

half of the mocks and find perfect match between the two results. This check ensures that our measurements of the covariance are accurate enough.

Combination with Planck data Combining Planck2018 with the BAO parameters we measured leads to the same results as Planck2018 combined with the BOSS DR12 consensus measurements [4].

wCDM fit Finally we check the theory-systematic error of our method on wCDM. In Fig. 8 and Table 6, we show the marginalized posterior distribution of the wCDM parameters with a BBN prior on ω_b , obtained by fitting the mean over 2048 CMASS NGC Patchy mocks,

FS	best-fit	mean $\pm \sigma$	FS+BAO	best-fit	mean $\pm \sigma$
ω_{cdm}	0.1294	$0.1369^{+0.011}_{-0.016}$	ω_{cdm}	0.1315	$0.1398^{+0.011}_{-0.016}$
H_0	68.96	$68.88^{+1.4}_{-1.8}$	H_0	68.94	$69.66^{+1.3}_{-1.6}$
$\ln \left(10^{10} A_s \right)$	2.871	$2.834^{+0.2}_{-0.21}$	$\ln \left(10^{10} A_s \right)$	2.852	$2.84^{+0.2}_{-0.21}$
n_s	0.908	$0.9134^{+0.077}_{-0.074}$	n_s	0.901	$0.9153^{+0.08}_{-0.08}$
$\Sigma m_{ u}$	0.1702	$0.3901^{+0.11}_{-0.33}$	$\Sigma m_{ u}$	0.2483	$0.4526^{+0.12}_{-0.39}$
σ_8	0.7484	$0.7217^{+0.045}_{-0.05}$	σ_8	0.733	$0.7258^{+0.045}_{-0.05}$

Table 5: Results on Λ CDM + massive neutrinos fitting BOSS FS (+ BAO) with a BBN prior on ω_b .

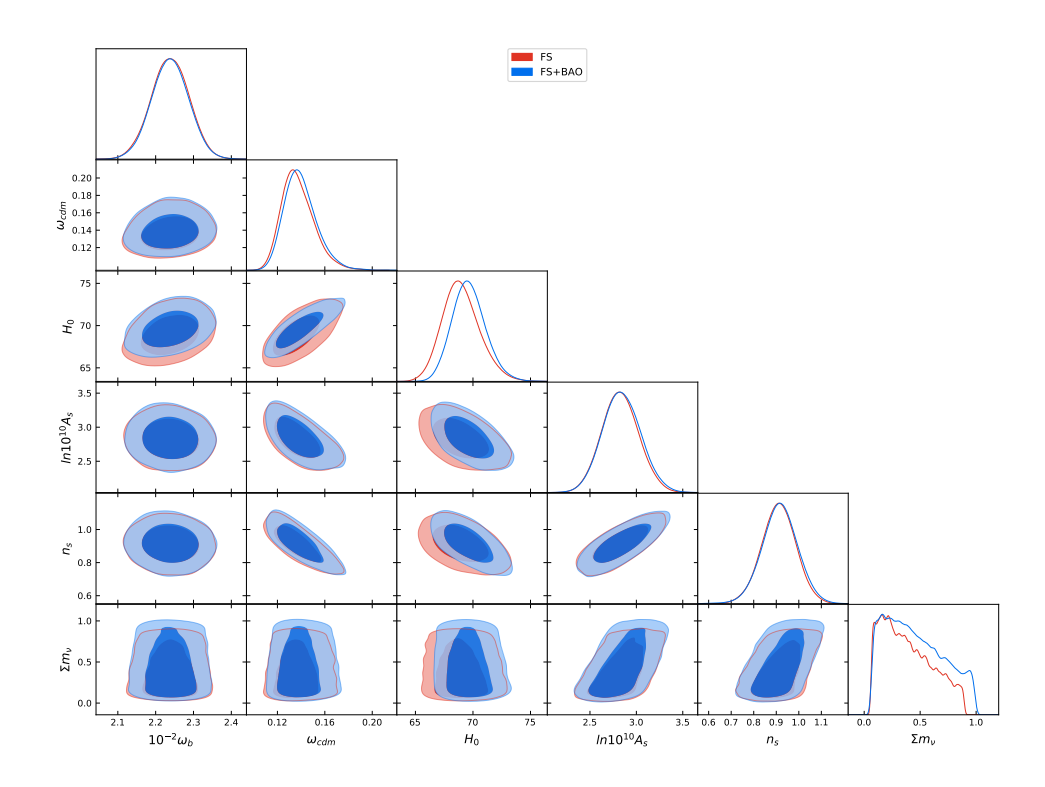


Figure 7: Triangle plot of Λ CDM + massive neutrinos fitting BOSS FS and BOSS FS + BAO with a BBN prior on ω_b .

analyzed with the covariance divided by 16. We also show there the results obtained by adding to the fit 'small-z' priors on r_s/D_V at $z_{\rm eff}=0.106$ and on D_V/r_s at $z_{\rm eff}=0.15$ similar to 6DF and SDSS DR7 MGS respectively, but with central value on the truth of the simulation and error bars rescaled by 4.

Let us discuss first the case without small-z. Inspecting the error bars, we can see that by measuring the theory-systematic error as the distance from the 68% confidence intervals of the 1D posteriors to the truth in the fit to the patchy mocks mean, we can detect a theory-systematic error within $\sim 1/3\sigma_{\rm stat}$ in the BOSS data. Although, with respect to the error bars obtained in the BOSS data, we detect no significant theory error, with at most a marginal one in $\ln(10^{10}A_s)$ of $\lesssim 1/3\sigma_{\rm stat}$, we observe that the trends in the shifts of the posteriors between Λ CDM (+ ν) and wCDM are similar for both patchy and BOSS data, resulting in slightly lower A_s and n_s , and slightly higher w_{cdm} and H_0 . This can be traced to the anti-correlations among wCDM in the FS+BAO analysis, as discussed in sec. 3. In particular, we find that w prefers, although not significantly, a lower value than -1, driving the trends we are observing.

Adding the small-z prior, we find that the posteriors are pushed towards the truth values, leading to even smaller theory errors, that become negligible. This is expected as adding another redshift help breaking degeneracies.

These tests on simulation allow us to confidently analyze wCDM on the observational data.

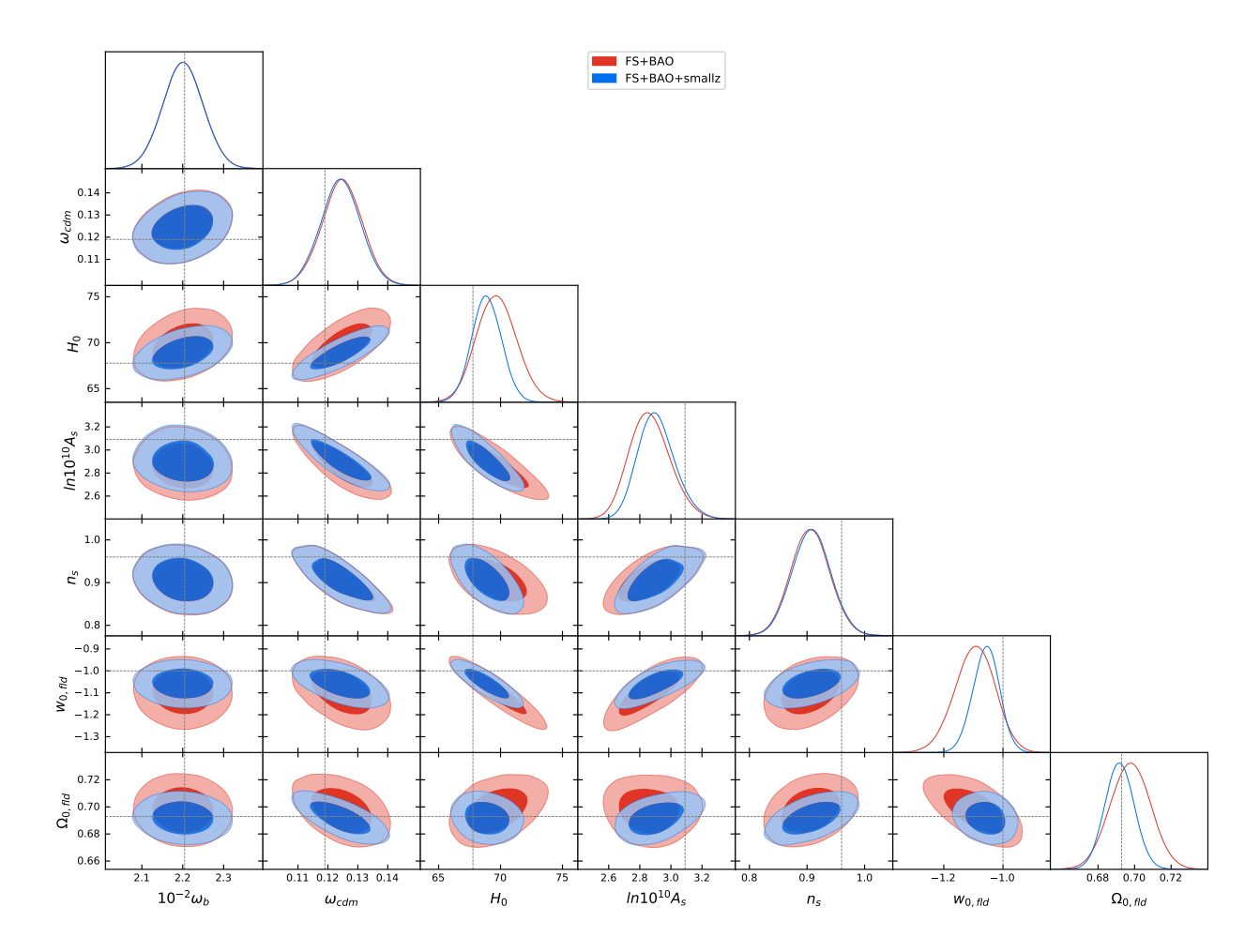


Figure 8: Triangle plot of wCDM fitting the mean of 2048 patchy CMASS NGC mocks FS + BAO with and without small-z, using a covariance rescaled by 16 and a BBN prior on ω_b .

B Marginalized likelihood and best fit

In this appendix, we explicitly show that even using the likelihood analytically marginalized over some of the EFT parameters one can recover with good accuracy their best fit values, necessary to recover the best fit power spectrum. We start by expressing the theory model as a sum of terms multiplied by EFT parameters appearing linearly plus all the other terms:

$$P_{\alpha} = \sum_{i} b_{G,i} P_{G,\alpha}^{i} + P_{NG,\alpha} . \tag{10}$$

Here we use a concise notation in which the index α runs over k-bins and multipoles; $b_{G,i}$ are the EFT parameters over which the marginalization is analytical, and both $P_{G,\alpha}^i$ and $P_{NG,\alpha}$ will depend on the cosmological parameters and the non-linear EFT parameters which cannot be analytically integrated out. The posterior can then be written as

$$-2\ln \mathcal{P} = (P_{\alpha} - D_{\alpha})C_{\alpha\beta}^{-1}(P_{\beta} - D_{\beta}) + b_{G,i}\sigma_{ij}^{-1}b_{G,j} - 2\ln\Pi,$$
(11)

FS+BAO	best-fit	mean $\pm \sigma$	truth	theory sys.	FS+BAO	best-fit	mean $\pm \sigma$	truth	theory sys.
${ m w/o~small-}z$				in $\sigma_{\rm data}$	m w/~small-z				in $\sigma_{\rm data}$
ω_{cdm}	0.1258	$0.1248^{+0.007}_{-0.0067}$	0.119	0%	ω_{cdm}	0.1248	$0.1243^{+0.0068}_{-0.0068}$	0.119	0%
H_0	69.6	$69.69^{+1.6}_{-1.7}$	67.77	5%	H_0	68.77	$68.88^{+1.2}_{-1.3}$	67.77	0%
$\ln\left(10^{10}A_s\right)$	2.841	$2.867^{+0.12}_{-0.15}$	3.091	35%	$\ln \left(10^{10} A_s \right)$	2.873	$2.908^{+0.11}_{-0.13}$	3.091	8%
n_s	0.9116	$0.9057^{+0.034}_{-0.035}$	0.96	25%	n_s	0.9175	$0.9077^{+0.034}_{-0.035}$	0.96	2%
$w_{0,fld}$	-1.086	$-1.095^{+0.072}_{-0.066}$	-1	10%	$w_{0,fld}$	-1.053	$-1.057^{+0.048}_{-0.046}$	-1	1%
$\Omega_{0,fld}$	0.695	$0.6977^{+0.012}_{-0.011}$	0.693	0%	$\Omega_{0,fld}$	0.6897	$0.6918^{+0.0083}_{-0.0084}$	0.693	0%

Table 6: Results on wCDM fitting the mean of 2048 patchy CMASS NGC mocks FS + BAO with and without small-z, using a covariance rescaled by 16 and a BBN prior on ω_b . The theory-systematic errors are quoted in percentage of the corresponding 68% confidence intervals, σ_{data} , obtained analyzing FS+BAO (BOSS) and FS+BAO (BOSS+small-z).

where D_{α} is the data vector, $C_{\alpha\beta}$ is the data covariance, and we introduced a Gaussian prior on the $b_{G,i}$ with covariance σ_{ij} , plus a generic prior Π on the cosmological and non-linear EFT parameters.

Collecting different powers of $b_{G,i}$, the posterior can be written in the form:

$$-2\ln \mathcal{P} = b_{G,i}F_{2,ij}b_{G,j} - 2b_{G,i}F_{1,i} + F_0,$$
(12)

where we defined the following terms:

$$F_{2,ij} = P_{G,\alpha}^i C_{\alpha\beta}^{-1} P_{G,\beta}^j + \sigma_{ij}^{-1} \,, \tag{13}$$

$$F_{1,i} = -P_{G\alpha}^{i} C_{\alpha\beta}^{-1} (P_{NG,\beta} - D_{\beta}), \qquad (14)$$

$$F_0 = (P_{NG,\alpha} - D_{\alpha})C_{\alpha\beta}^{-1}(P_{NG,\beta} - D_{\beta}) - 2\ln\Pi.$$
 (15)

Performing a Gaussian integral on the $b_{G,i}$, we obtain the marginalized posterior:

$$-2\ln \mathcal{P}_{\text{marg}} = -F_{1,i}F_{2,ij}^{-1}F_{1,j} + F_0 + \ln \det \left(\frac{F_2}{2\pi}\right). \tag{16}$$

We will now show the relation between the extrema of eq. (12) and of eq. (16). Setting the gradients of eq. (12) to zero we find:

$$b_{G,i} = F_{2,ij}^{-1} F_{1,j} , (17)$$

$$b_{G,i} \frac{\partial F_{2,ij}}{\partial c_n} b_{G,j} - 2b_{G,i} \frac{\partial F_{1,i}}{\partial c_n} + \frac{\partial F_0}{\partial c_n} = 0,$$

$$(18)$$

where c_n is any other parameter we want to fit. The first equation is already solved in terms of the c_n . Substituting into the second, we find the nonlinear equation which determines the best fit for the c_n using the non-marginalized likelihood:

$$0 = F_{1,k} F_{2,ik}^{-1} \frac{\partial F_{2,ij}}{\partial c_n} F_{2,jl}^{-1} F_{1,l} - 2 \frac{\partial F_{1,i}}{\partial c_n} F_{2,ij}^{-1} F_{1,j} + \frac{\partial F_0}{\partial c_n}$$

$$= -F_{1,i} \frac{\partial F_{2,ij}^{-1}}{\partial c_n} F_{1,j} - 2 \frac{\partial F_{1,i}}{\partial c_n} F_{2,ij}^{-1} F_{1,j} + \frac{\partial F_0}{\partial c_n},$$
(19)

where we used the fact that $F_{2,ij}$ is symmetric and we expressed its derivative in terms of the derivative of its inverse.

If we instead start from eq. (16), to find the best fit, we can use eq. (17) for the $b_{G,i}$'s best fit, while the best fit of the c_n parameters is given by the solution of the following equation:

$$-F_{1,i}\frac{\partial F_{2,ij}^{-1}}{\partial c_n}F_{1,j} - 2\frac{\partial F_{1,i}}{\partial c_n}F_{2,ij}^{-1}F_{1,j} + \frac{\partial F_0}{\partial c_n} + F_{2,ji}^{-1}\frac{\partial F_{2,ji}}{\partial c_n} = 0.$$
 (20)

Because of the last term, the best fit point using the marginalized posterior is shifted with respect to the best fit point obtained from the non-marginalized posterior.

However, this term is generically small. To get an idea of the size of the various terms, let us consider a single b_G and a single k-bin. We can estimate the size of the last and the first terms as $F_2^{-1} \frac{\partial F_2}{\partial c_n} \sim P_G^{-1} \frac{\partial F_G}{\partial c_n}$, $F_1 \frac{\partial F_2^{-1}}{\partial c_n} F_1 \sim \frac{(P_{NG} - D)^2}{P_G} C^{-1} \frac{\partial P_G}{\partial c_n}$. Therefore

$$\left| \frac{F_{2,ji}^{-1} \frac{\partial F_{2,ji}}{\partial c_n}}{F_{1,i} \frac{\partial F_{2,ij}^{-1}}{\partial c_n} F_{1,j}} \right| \sim \frac{C}{(P_{NG} - D)^2}. \tag{21}$$

Now, $(P_{NG} - D)^2$ is of the size of the one-loop squared, while C is the squared error on the data, which at k_{max} is of order of the two-loop squared, therefore the r.h.s. is negligible.

In practice, we find that the best fits from the marginalized posterior and from the non-marginalized posterior are equal to better than 0.1% precision on all parameters for all analyses we performed on data or simulations.

References

- [1] The Cosmological Analysis of the SDSS/BOSS data from the Effective Field Theory of Large-Scale Structure, 1909.05271.
- [2] M. M. Ivanov, M. Simonović and M. Zaldarriaga, Cosmological Parameters from the BOSS Galaxy Power Spectrum, 1909.05277.
- [3] T. Colas, G. D'amico, L. Senatore, P. Zhang and F. Beutler, Efficient Cosmological Analysis of the SDSS/BOSS data from the Effective Field Theory of Large-Scale Structure, 1909.07951.
- [4] Planck collaboration, N. Aghanim et al., *Planck 2018 results. VI. Cosmological parameters*, 1807.06209.
- [5] A. G. Riess, S. Casertano, W. Yuan, L. M. Macri and D. Scolnic, Large Magellanic Cloud Cepheid Standards Provide a 1% Foundation for the Determination of the Hubble Constant and Stronger Evidence for Physics beyond ΛCDM, Astrophys. J. 876 (2019) 85, [1903.07603].

- [6] L. Verde, T. Treu and A. G. Riess, Tensions between the Early and the Late Universe, in Nature Astronomy 2019, 2019. 1907.10625. DOI.
- [7] D. Baumann, A. Nicolis, L. Senatore and M. Zaldarriaga, Cosmological Non-Linearities as an Effective Fluid, JCAP 1207 (2012) 051, [1004.2488].
- [8] J. J. M. Carrasco, M. P. Hertzberg and L. Senatore, The Effective Field Theory of Cosmological Large Scale Structures, JHEP 09 (2012) 082, [1206.2926].
- [9] R. A. Porto, L. Senatore and M. Zaldarriaga, *The Lagrangian-space Effective Field Theory of Large Scale Structures*, *JCAP* **1405** (2014) 022, [1311.2168].
- [10] J. J. M. Carrasco, S. Foreman, D. Green and L. Senatore, *The 2-loop matter power spectrum and the IR-safe integrand*, *JCAP* **1407** (2014) 056, [1304.4946].
- [11] J. J. M. Carrasco, S. Foreman, D. Green and L. Senatore, *The Effective Field Theory of Large Scale Structures at Two Loops*, *JCAP* **1407** (2014) 057, [1310.0464].
- [12] S. M. Carroll, S. Leichenauer and J. Pollack, Consistent effective theory of long-wavelength cosmological perturbations, Phys. Rev. D90 (2014) 023518, [1310.2920].
- [13] L. Senatore and M. Zaldarriaga, The IR-resummed Effective Field Theory of Large Scale Structures, JCAP 1502 (2015) 013, [1404.5954].
- [14] T. Baldauf, E. Schaan and M. Zaldarriaga, On the reach of perturbative methods for dark matter density fields, JCAP 1603 (2016) 007, [1507.02255].
- [15] S. Foreman, H. Perrier and L. Senatore, *Precision Comparison of the Power Spectrum* in the EFTofLSS with Simulations, JCAP **1605** (2016) 027, [1507.05326].
- [16] T. Baldauf, L. Mercolli and M. Zaldarriaga, Effective field theory of large scale structure at two loops: The apparent scale dependence of the speed of sound, Phys. Rev. D92 (2015) 123007, [1507.02256].
- [17] M. Cataneo, S. Foreman and L. Senatore, Efficient exploration of cosmology dependence in the EFT of LSS, 1606.03633.
- [18] M. Lewandowski and L. Senatore, IR-safe and UV-safe integrands in the EFTofLSS with exact time dependence, JCAP 1708 (2017) 037, [1701.07012].
- [19] T. Konstandin, R. A. Porto and H. Rubira, *The Effective Field Theory of Large Scale Structure at Three Loops*, 1906.00997.
- [20] E. Pajer and M. Zaldarriaga, On the Renormalization of the Effective Field Theory of Large Scale Structures, JCAP 1308 (2013) 037, [1301.7182].

- [21] A. A. Abolhasani, M. Mirbabayi and E. Pajer, Systematic Renormalization of the Effective Theory of Large Scale Structure, JCAP 1605 (2016) 063, [1509.07886].
- [22] L. Mercolli and E. Pajer, On the velocity in the Effective Field Theory of Large Scale Structures, JCAP 1403 (2014) 006, [1307.3220].
- [23] M. McQuinn and M. White, Cosmological perturbation theory in 1+1 dimensions, JCAP **1601** (2016) 043, [1502.07389].
- [24] L. Senatore, Bias in the Effective Field Theory of Large Scale Structures, JCAP 1511 (2015) 007, [1406.7843].
- [25] L. Senatore and M. Zaldarriaga, Redshift Space Distortions in the Effective Field Theory of Large Scale Structures, 1409.1225.
- [26] T. Baldauf, M. Mirbabayi, M. Simonovic and M. Zaldarriaga, Equivalence Principle and the Baryon Acoustic Peak, Phys. Rev. **D92** (2015) 043514, [1504.04366].
- [27] L. Senatore and G. Trevisan, On the IR-Resummation in the EFTofLSS, JCAP 1805 (2018) 019, [1710.02178].
- [28] M. Lewandowski and L. Senatore, An analytic implementation of the IR-resummation for the BAO peak, 1810.11855.
- [29] D. Blas, M. Garny, M. M. Ivanov and S. Sibiryakov, Time-Sliced Perturbation Theory II: Baryon Acoustic Oscillations and Infrared Resummation, JCAP 1607 (2016) 028, [1605.02149].
- [30] M. Lewandowski, A. Perko and L. Senatore, Analytic Prediction of Baryonic Effects from the EFT of Large Scale Structures, JCAP 1505 (2015) 019, [1412.5049].
- [31] R. E. Angulo, S. Foreman, M. Schmittfull and L. Senatore, The One-Loop Matter Bispectrum in the Effective Field Theory of Large Scale Structures, JCAP 1510 (2015) 039, [1406.4143].
- [32] T. Baldauf, L. Mercolli, M. Mirbabayi and E. Pajer, *The Bispectrum in the Effective Field Theory of Large Scale Structure*, *JCAP* **1505** (2015) 007, [1406.4135].
- [33] D. Bertolini, K. Schutz, M. P. Solon and K. M. Zurek, *The Trispectrum in the Effective Field Theory of Large Scale Structure*, 1604.01770.
- [34] T. Baldauf, E. Schaan and M. Zaldarriaga, On the reach of perturbative descriptions for dark matter displacement fields, JCAP 1603 (2016) 017, [1505.07098].
- [35] S. Foreman and L. Senatore, The EFT of Large Scale Structures at All Redshifts: Analytical Predictions for Lensing, JCAP 1604 (2016) 033, [1503.01775].

- [36] M. Mirbabayi, F. Schmidt and M. Zaldarriaga, Biased Tracers and Time Evolution, JCAP 1507 (2015) 030, [1412.5169].
- [37] R. Angulo, M. Fasiello, L. Senatore and Z. Vlah, On the Statistics of Biased Tracers in the Effective Field Theory of Large Scale Structures, JCAP 1509 (2015) 029, [1503.08826].
- [38] T. Fujita, V. Mauerhofer, L. Senatore, Z. Vlah and R. Angulo, Very Massive Tracers and Higher Derivative Biases, 1609.00717.
- [39] A. Perko, L. Senatore, E. Jennings and R. H. Wechsler, *Biased Tracers in Redshift Space in the EFT of Large-Scale Structure*, 1610.09321.
- [40] E. O. Nadler, A. Perko and L. Senatore, On the Bispectra of Very Massive Tracers in the Effective Field Theory of Large-Scale Structure, JCAP 1802 (2018) 058, [1710.10308].
- [41] P. McDonald and A. Roy, Clustering of dark matter tracers: generalizing bias for the coming era of precision LSS, JCAP 0908 (2009) 020, [0902.0991].
- [42] M. Lewandowski, L. Senatore, F. Prada, C. Zhao and C.-H. Chuang, *EFT of large scale structures in redshift space*, *Phys. Rev.* **D97** (2018) 063526, [1512.06831].
- [43] L. Senatore and M. Zaldarriaga, The Effective Field Theory of Large-Scale Structure in the presence of Massive Neutrinos, 1707.04698.
- [44] R. de Belsunce and L. Senatore, Tree-Level Bispectrum in the Effective Field Theory of Large-Scale Structure extended to Massive Neutrinos, 1804.06849.
- [45] M. Lewandowski, A. Maleknejad and L. Senatore, An effective description of dark matter and dark energy in the mildly non-linear regime, JCAP 1705 (2017) 038, [1611.07966].
- [46] G. Cusin, M. Lewandowski and F. Vernizzi, Dark Energy and Modified Gravity in the Effective Field Theory of Large-Scale Structure, JCAP 1804 (2018) 005, [1712.02783].
- [47] B. Bose, K. Koyama, M. Lewandowski, F. Vernizzi and H. A. Winther, *Towards Precision Constraints on Gravity with the Effective Field Theory of Large-Scale Structure*, *JCAP* **1804** (2018) 063, [1802.01566].
- [48] V. Assassi, D. Baumann, E. Pajer, Y. Welling and D. van der Woude, Effective theory of large-scale structure with primordial non-Gaussianity, JCAP 1511 (2015) 024, [1505.06668].
- [49] V. Assassi, D. Baumann and F. Schmidt, Galaxy Bias and Primordial Non-Gaussianity, JCAP 1512 (2015) 043, [1510.03723].

- [50] D. Bertolini, K. Schutz, M. P. Solon, J. R. Walsh and K. M. Zurek, Non-Gaussian Covariance of the Matter Power Spectrum in the Effective Field Theory of Large Scale Structure, 1512.07630.
- [51] D. Bertolini and M. P. Solon, Principal Shapes and Squeezed Limits in the Effective Field Theory of Large Scale Structure, 1608.01310.
- [52] M. Simonovic, T. Baldauf, M. Zaldarriaga, J. J. Carrasco and J. A. Kollmeier, Cosmological perturbation theory using the FFTLog: formalism and connection to QFT loop integrals, JCAP 1804 (2018) 030, [1708.08130].
- [53] H. Gil-Marín et al., The clustering of galaxies in the SDSS-III Baryon Oscillation Spectroscopic Survey: RSD measurement from the LOS-dependent power spectrum of DR12 BOSS galaxies, Mon. Not. Roy. Astron. Soc. 460 (2016) 4188–4209, [1509.06386].
- [54] H. Gil-Marín et al., The clustering of galaxies in the SDSS-III Baryon Oscillation Spectroscopic Survey: BAO measurement from the LOS-dependent power spectrum of DR12 BOSS galaxies, Mon. Not. Roy. Astron. Soc. 460 (2016) 4210–4219, [1509.06373].
- [55] D. M. Scolnic et al., The Complete Light-curve Sample of Spectroscopically Confirmed SNe Ia from Pan-STARRS1 and Cosmological Constraints from the Combined Pantheon Sample, Astrophys. J. 859 (2018) 101, [1710.00845].
- [56] F. Beutler, C. Blake, M. Colless, D. H. Jones, L. Staveley-Smith, L. Campbell et al., The 6dF Galaxy Survey: Baryon Acoustic Oscillations and the Local Hubble Constant, Mon. Not. Roy. Astron. Soc. 416 (2011) 3017–3032, [1106.3366].
- [57] A. J. Ross, L. Samushia, C. Howlett, W. J. Percival, A. Burden and M. Manera, The clustering of the SDSS DR7 main Galaxy sample I. A 4 per cent distance measure at z = 0.15, Mon. Not. Roy. Astron. Soc. 449 (2015) 835–847, [1409.3242].
- [58] V. de Sainte Agathe et al., Baryon acoustic oscillations at z=2.34 from the correlations of Ly α absorption in eBOSS DR14, Astron. Astrophys. **629** (2019) A85, [1904.03400].
- [59] M. Blomqvist et al., Baryon acoustic oscillations from the cross-correlation of Lyα absorption and quasars in eBOSS DR14, Astron. Astrophys. 629 (2019) A86, [1904.03430].
- [60] O. H. E. Philcox, M. M. Ivanov, M. Simonović and M. Zaldarriaga, Combining Full-Shape and BAO Analyses of Galaxy Power Spectra: A 1.6% CMB-independent constraint on H0, 2002.04035.

- [61] DES collaboration, T. M. C. Abbott et al., Dark Energy Survey year 1 results: Cosmological constraints from galaxy clustering and weak lensing, Phys. Rev. D98 (2018) 043526, [1708.01530].
- [62] DES collaboration, T. M. C. Abbott et al., Cosmological Constraints from Multiple Probes in the Dark Energy Survey, Phys. Rev. Lett. 122 (2019) 171301, [1811.02375].
- [63] BOSS collaboration, S. Alam et al., The clustering of galaxies in the completed SDSS-III Baryon Oscillation Spectroscopic Survey: cosmological analysis of the DR12 galaxy sample, Mon. Not. Roy. Astron. Soc. 470 (2017) 2617–2652, [1607.03155].
- [64] T. Brinckmann and J. Lesgourgues, MontePython 3: boosted MCMC sampler and other features, 1804.07261.
- [65] B. Audren, J. Lesgourgues, K. Benabed and S. Prunet, Conservative Constraints on Early Cosmology: an illustration of the Monte Python cosmological parameter inference code, JCAP 1302 (2013) 001, [1210.7183].
- [66] A. Cuceu, J. Farr, P. Lemos and A. Font-Ribera, Baryon Acoustic Oscillations and the Hubble Constant: Past, Present and Future, JCAP 1910 (2019) 044, [1906.11628].
- [67] R. J. Cooke, M. Pettini and C. C. Steidel, One Percent Determination of the Primordial Deuterium Abundance, Astrophys. J. 855 (2018) 102, [1710.11129].
- [68] M. M. Ivanov, M. Simonović and M. Zaldarriaga, Cosmological Parameters and Neutrino Masses from the Final Planck and Full-Shape BOSS Data, 1912.08208.
- [69] 2DFGRS TEAM collaboration, W. J. Percival et al., Parameter constraints for flat cosmologies from CMB and 2dFGRS power spectra, Mon. Not. Roy. Astron. Soc. 337 (2002) 1068, [astro-ph/0206256].
- [70] V. F. Mukhanov, CMB-slow, or how to estimate cosmological parameters by hand, Int. J. Theor. Phys. 43 (2004) 623–668, [astro-ph/0303072].
- [71] A. J. S. Hamilton, Uncorrelated modes of the nonlinear power spectrum, Mon. Not. Roy. Astron. Soc. 312 (2000) 257–284, [astro-ph/9905191].
- [72] C. Howlett, A. Lewis, A. Hall and A. Challinor, CMB power spectrum parameter degeneracies in the era of precision cosmology, JCAP 1204 (2012) 027, [1201.3654].
- [73] D. Blas, J. Lesgourgues and T. Tram, The Cosmic Linear Anisotropy Solving System (CLASS) II: Approximation schemes, JCAP 1107 (2011) 034, [1104.2933].
- [74] S. van der Walt, S. C. Colbert and G. Varoquaux, *The numpy array: A structure for efficient numerical computation*, *Computing in Science Engineering* **13** (March, 2011) 22–30.

- [75] P. Virtanen, R. Gommers, T. E. Oliphant, M. Haberland, T. Reddy, D. Cournapeau et al., SciPy 1.0: Fundamental Algorithms for Scientific Computing in Python, Nature Methods (2020).
- [76] J. E. McEwen, X. Fang, C. M. Hirata and J. A. Blazek, FAST-PT: a novel algorithm to calculate convolution integrals in cosmological perturbation theory, 1603.04826.
- [77] D. Blas, J. Lesgourgues and T. Tram, The cosmic linear anisotropy solving system (CLASS). part II: Approximation schemes, Journal of Cosmology and Astroparticle Physics **2011** (jul, 2011) 034–034.
- [78] F. Beutler, E. Castorina and P. Zhang, Interpreting measurements of the anisotropic galaxy power spectrum, 1810.05051.
- [79] BOSS collaboration, F. Beutler et al., The clustering of galaxies in the completed SDSS-III Baryon Oscillation Spectroscopic Survey: baryon acoustic oscillations in the Fourier space, Mon. Not. Roy. Astron. Soc. 464 (2017) 3409–3430, [1607.03149].